Kinematic Study of Human Ankle Control During Walking

by

Julia C. Zimmerman

SUBMITTED TO THE DEPARTMENT OF MECHANICAL ENGINEERING IN PARTIAL FULFILLMENT OF THE REQUIREMENTS FOR THE DEGREE OF

BACHELOR OF SCIENCE IN MECHANICAL ENGINEERING
AT THE
MASSACHUSETTS INSTITUTE OF TECHNOLOGY

JUNE 2009

Signature of Author_____
Department of Mechanical Engineering
May 8, 2009

Certified by:_____
Professor N. Hogan
Professor of Mechanical Engineering
Professor of Brain and Cognitive Sciences
Thesis Supervisor

Accepted by:_____
Professor J. Lienhard V
Collins Professor of Mechanical Engineering
Chairman, Undergraduate Thesis Committee

Kinematic Study of Human Ankle Control During Walking

by

Julia C. Zimmerman

Submitted to the Department of Mechanical Engineering
on May 8, 2009 in Partial Fulfillment of the
Requirements for the Degree of Bachelor of Science in
Mechanical Engineering

ABSTRACT

In order to determine the extent to which ankle motion is voluntarily controlled during walking, angular velocity measurements at the ankle were taken in two cases. In the first case, subjects were seated and instructed to move their ankle as quickly as possible in eight directions indicated by a computer program in dorsi- and plantar-flexion and inversion and eversion. In the second case, subjects were instructed to walk on a treadmill for thirty seconds at a normal pace, and at speeds that felt faster and slower than normal. Velocity measurements were made using an exoskeletal robot, called the Anklebot, originally designed for rehabilitation purposes. The electromyogram of anterior tibialis, peroneus longus, and gastrocnemius muscles was also recorded. Results showed that all subjects plantarflexed their foot at a higher velocity after heel-strike while walking than when moving at their maximum voluntary speed. This implies that this motion results in part from foot-ground interaction mediated by the mechanical impedance of the ankle and is not solely imposed by contraction of the gastrocnemius and other muscles. In contrast, results also showed that subjects were able to dorsiflex their foot at a higher velocity when moving at maximum voluntary speed than was observed after toe-off while walking.

Thesis Supervisor: Neville Hogan
Title: Professor of Mechanical Engineering, Professor of Brain and Cognitive Sciences

ACKNOWLEDGEMENTS

First and foremost, I would like to thank Prof. Neville Hogan for including me in his research at the Newman Lab for Biomechanics and Human Rehabilitation. I have greatly enjoyed the opportunity to work with such talented researchers.

I would also like to thank Patrick Ho for his guidance throughout my time in the Newman Lab and for teaching me how to use the tools necessary to complete my research.

Lastly, I would like to thank my family and friends for all the support and love they've given me and for always believing in me.

TABLE OF CONTENTS

LIST OF FIGURES

LIST OF TABLES

INTRODUCTION

For centuries, scientists have been striving to understand human anatomy and how the human body works mechanically. In recent years, more significant means of measurement have allowed greater insight into how the body moves. The aim of this project was to use modern means of measurement to determine whether ankle motion during walking is controlled voluntarily or arises from the mechanics of foot-ground interaction mediated by ankle mechanical impedance. A device, called the Anklebot, was used to measure the position and velocity of the ankle with respect to the shank during rapid voluntary ankle movements as well as while the subject was walking on a treadmill at various speeds. Also, the electrical activity or electromyogram (EMG) of muscles associated with ankle movement was measured in order to compare how a person recruits muscles during voluntary movements and while walking. This information was used to infer how individuals control ankle movement while walking.

1.1 Motivation

A thorough understanding of how the human body works is a necessity in providing better medical treatment for a range of ailments. For example, "drop foot" is a condition resulting in a patient's inability to raise the front of the foot due to weakness or paralysis of the muscles that lift the foot. Drop foot results from a variety of conditions, including stroke, multiple sclerosis, and polio [1]. In order to treat patients suffering from drop foot through either rehabilitation or orthotics, it

is necessary to understand as thoroughly as possible the workings of the ankle and how its motion is controlled in a healthy individual.

Additionally, a clear understanding of the kinematics of the human ankle is critical in designing prosthetic feet that more precisely mimic a real human foot. For amputees, walking with a prosthetic foot can lead to other health problems, such as severe back pains and arthritis, due to improper fit and alignment and postural changes [11]. In order to provide amputees with the best care possible, it is important to learn as much as possible about the human ankle and foot and how it is controlled in a healthy individual.

In a more indirect way, a better understanding of the body's kinematics could be useful in diagnosing injuries that simple x-rays or even more advanced imaging techniques, such as magnetic resonance imaging (MRI), might not be able to diagnose. By analyzing an unhealthy patient's movements and comparing them to those of a healthy person, it may be possible to determine where the injury is, how it is affecting the patient, and what may be the best way to treat the patient. This will only be possible with a more thorough understanding of the body's kinematics and how it relates to certain ailments.

In addition to researching human motion for medical reasons, this information could also be used to improve the design of humanoid robots. Currently, human gait can be described by nine gait determinants: pelvic rotation, pelvic tilt, knee flexion during stance phase, controlled plantar flexion, powered plantar flexion, lateral displacement of the pelvis, inversion-eversion-inversion at the subtalar joint, lateral flexion of the trunk, and anteroposterior flexion of the trunk [2]. Understanding

what these motions are is just the first step in determining how and why they come about. Current humanoid robots, such as Honda's Asimo and the Kawada HRP-2, have gaits that appear human-like, but only satisfy a few of these gait determinants. A better understanding of joint kinematics and how these gait determinants are controlled by an individual will lead to an improvement in our ability to mimic human motion with robotics.

The ankle is a complex joint, whose motion has a great impact on many daily activities. A more complete understanding of how the ankle is controlled during walking would be useful both to provide better treatment for patients with walking disabilities and to more precisely mimic walking motions with prosthetic or robotic devices. This project aims to gain insight into human control of walking through an analysis of the kinematics of the ankle during rapid voluntary ankle movements, comparing these measurements to the motions of the ankle during walking at various speeds.

1.2 Social and Ethical Implications

As with many scientific discoveries, the knowledge gained through this project could be used to improve lives as well as harm others. The knowledge could be used to improve patient care for persons suffering paralysis after stroke or from neurological disease. A better understanding of ankle kinematics could also be used to improve the design of humanoid robots that will replace humans in dangerous situations and potentially save lives. As with many machines, these humanoid robots could also potentially be used as weapons and cause more destruction than

good. Yet, in the right hands, knowledge of the workings of the human body is an asset for doctors and others who work to improve the lives of individuals with disabilities.

2.0 LITERATURE REVIEW

Before discussing models of the human ankle and its mechanics, it is useful to have a basic understanding of the anatomical structures of the foot, as shown in Figure 1. The talus is the central bone of the ankle, and together with the tibia and fibula of the shank comprises the upper ankle joint. This joint allows primarily planar rotation in plantarflexion and dorsiflexion with a range of motion of about 45°, divided equally between plantar and dorsiflexion. The lower part of the talus articulates with both the calcaneous and the navicular at the talocalcaneal joint and talonavicular joint respectively. The cuboid also articulates with the navicular and the calcaneous. Because the motion of these four joints can be modeled as a closed kinematic chain with one degree of freedom, the motion of these four joints is regarded as planar motion about one axis at the subtalar joint. The range of motion is about 25°, 20° inversion and 5° eversion [4].

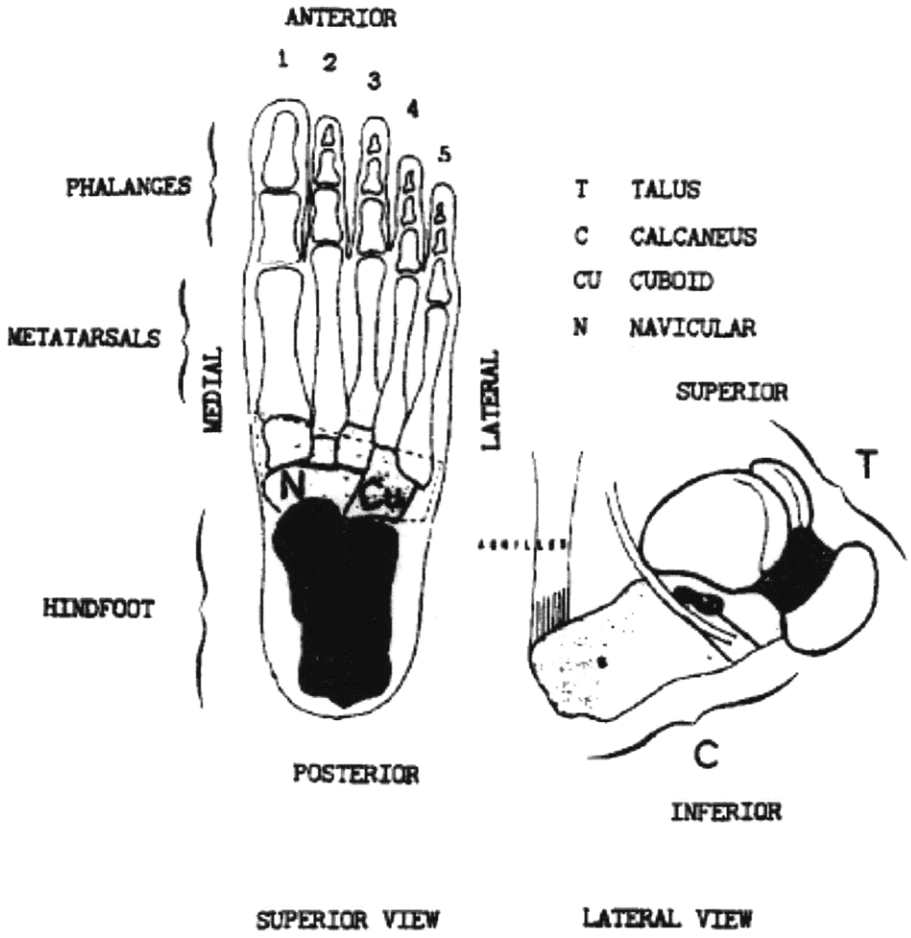

Figure 1: Anatomy of the human ankle and foot [5].

2.1 Kinematic Models of the Human Ankle

Because of the critical role that the human ankle plays in physical activities, several models have been developed in order to describe its motions. These models are useful for developing the better understanding necessary for many medical applications, including performing total ankle replacement and ligament reconstruction [3]. Early kinematic models used to describe the motion between the shank and the foot described it as a hinge joint (revolute joint) that represents dorsiflexion/plantarflexion. This only allowed planar motion with one degree of freedom. Other models described the motion of the ankle using a ball and socket

joint (spherical joint). This model has three rotational degrees of freedom, but assumes that all points of the foot move in concentric spheres about the joint center, which does not accurately describe the physiological rotations of plantarflexion/dorsiflexion and inversion/eversion [4].

Dul and Johnson [4] modeled the ankle as two hinge joints, one at the upper ankle joint (between the shank and the talus) and one at the subtalar joint (between the talus and the foot). Rotation about the upper ankle joint, φ_u, represents dorsiflexion and plantarflexion, and rotation about the subtalar joint, φ_l, represents inversion and eversion as shown in Figure 2.

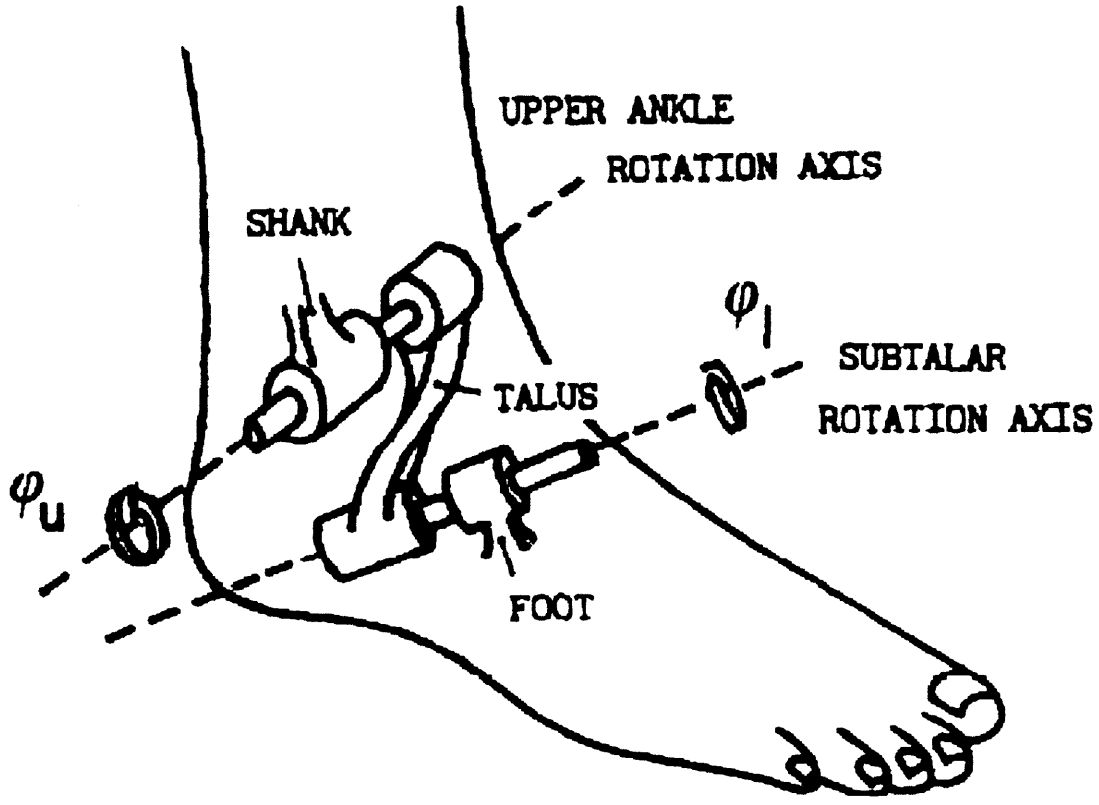

Figure 2: A kinematic model of the human ankle modeled as a system of three rigid links (shank, talus, and foot) connected by two hinge joints [4].

Using this model, Dul and Johnson [4] created a 4x4 transformation matrix to describe the relationship between a coordinate system fixed to the foot and a coordinate system fixed to the shank. Using this transformation matrix allowed a point on the foot to be expressed in coordinates relative to the shank. This model can be used for posture and motion simulations or as an aid in the design of ankle prostheses.

Dul and Johnson's model, although an improvement upon earlier models, makes the assumption that the foot has no toes, no joints distal to the ankle, no viscoelastic plantar tissue, nor any spatial characteristics in the mediolateral axis. Scott and Winter [6] attempt to remedy this in their model of the human ankle. In their model, the plantar soft tissue is modeled as a set of seven springs and dampers in parallel, accounting for the nature of the viscoelastic plantar tissue. The intertarsal joints, which are often overlooked in the literature, are considered in this model. Motion between the hind- and mid-foot regions occurs at the transverse tarsal joint, which is created by the talonavicular and calcaneocuboid joints. Other intertarsal joints are surrounded by tight ligamentous structures and provide only small motions compared to the transverse tarsal joint, so they have been neglected in this model. Because motion between the second metatarsal and the tarsal is limited, it is assumed to be a rigid joint, whereas the motion of the first, third, fourth, and fifth metatarsals are considered independent from tarsal motion.

2.2 Measurement Methods for the Ankle Joint

Although simplified models are useful to develop a better understanding of how the ankle moves, even more insight can be gained through actual measurements on a healthy ankle. One such measurement device was developed by Giacomozzi et al [7] to detect foot displacement with respect to the shank and torques or moments at the ankle articular complex. As shown in Figure 3, this measurement device consists of a six degrees-of-freedom chain comprising seven links that are connected through three revolute joints and three prismatic joints. The subject is seated with the foot fixed to plate 6 and the leg tied to a fork-shaped support rigidly fixed to the base link 0.

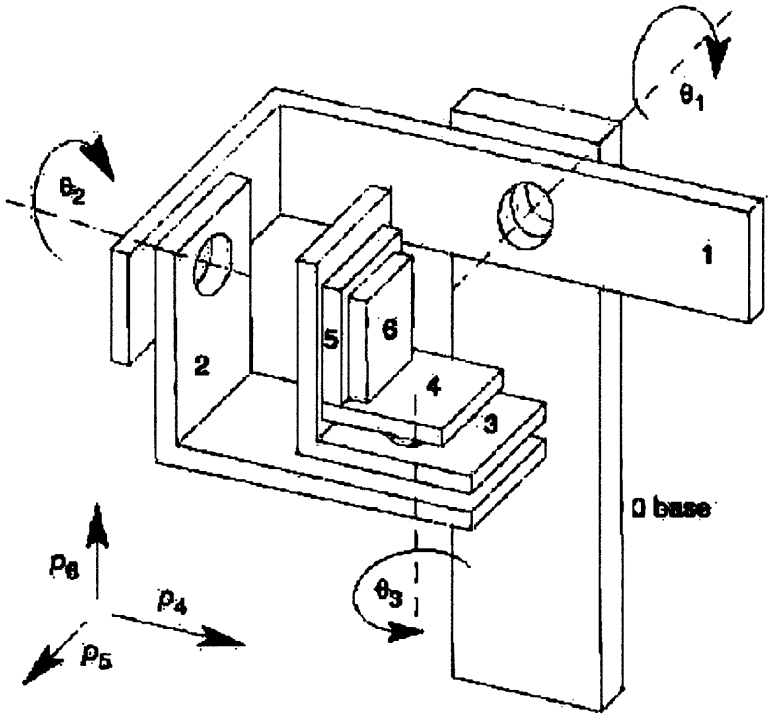

Figure 3: Diagram representing the seven links of the 6 DOF chain. Link 0 is rigidly attached to the subject's leg. Link 6 is rigidly attached to the subject's foot.

Using this device, Giacomozzi et al [7] were able to measure the maximum voluntary contraction (MVC) of several healthy subjects in various degrees of dorsiflexion/plantarflexion and inversion/eversion. Torques were measured using extensometric bridges mounted so as to transduce the torsional strain on the shafts of the three revolute joints. Joint angles were measured using continuous rotation precision potentiometers. Although this device is useful for measuring ankle motions while in a sitting position, it cannot be used while walking. Measurements of the ankle while walking are critical in understanding how the ankle functions for applications such as prosthetics and robotics.

2.3 Mechanics of the Ankle Joint While Walking

Measurements of the ankle in the sitting position are useful for determining the mechanics of the foot itself, but in order to best understand how the foot operates during locomotion, measurements need to be taken while the subject is walking. In David Winter's study [8] of lower limb gait during walking, reflective markers were attached to relevant anatomical landmarks: toe, metatarsolphalangeal joint, heel, ankle, lateral head of fibula, lateral epicondyle of femur, greater trochanter, iliac crest, and mid-trunk region. The coordinates of the body and background markers were recorded via video camera and used to determine limb position [8]. Force plate data was also recorded. From this, Winter was able to find joint angular positions at various velocities, as shown in Figure 4 [9].

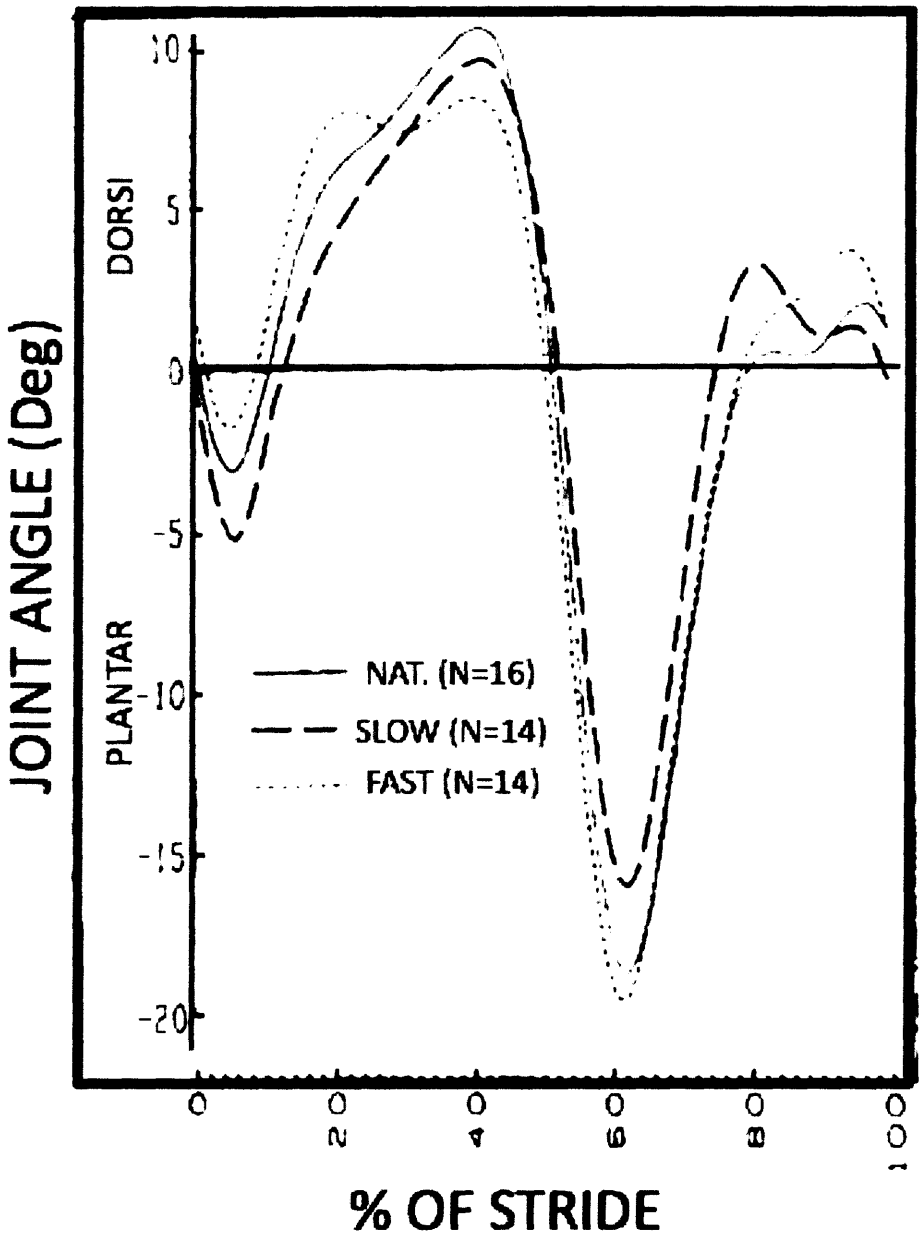

Figure 4: Mean ankle angle for each cadence group during stride cycle. Fast and slow cadences are defined as 20 steps/minute more or less than the natural cadence, respectively. Heel strike occurs a 0% of stride; toe off occurs at 60% of stride.

This method only captures motion in the sagittal plane, ignoring motion such as inversion and eversion of the ankle, which may be important in locomotion.

The methods discussed above have been used in the past to create accurate models of the ankle and its kinematics, but focus on kinematics either only while sitting or only while walking. This project aims to observe both states, comparing and contrasting relevant factors.

3.0 METHODS

3.1 Anklebot

The Anklebot [10], a three degrees-of-freedom wearable robot pictured in Figure 5, was originally designed as a rehabilitation aid for patients suffering from drop foot. Despite being designed for rehabilitation, the Anklebot can also be used to measure intrinsic ankle properties. The robot allows motion in all three degrees of freedom of the foot relative to the shank and can be worn while walking on ground, on a treadmill, or sitting in a chair. It also provides actuation in plantar-dorsiflexion (when the two links move in the same direction) and inversion-eversion (when the two links move in opposite directions) using two linear actuators mounted in parallel. The Anklebot allows 25° of dorsiflexion, 45° of plantarflexion, 25° of inversion, and 20° of eversion and can deliver a continuous torque of 17 N-m and a peak torque of ~40 N-m. Sensors include 2 rotary encoders and 2 linear incremental encoders. The rotary encoders have a resolution of 8.78×10^{-3} deg and are used to commutate the motors; the linear encoders have a resolution of 5×10^{-6} m and are used to measure the length of the actuators and

provide feedback to the controller. From the measured actuator lengths, geometrical and anthropometric data are used to determine joint angles and velocities [10]. A computer program created to log data of all experiments using the Anklebot handles the calculations required to find joint velocities from joint angles at consecutive time steps sampled at 200Hz.

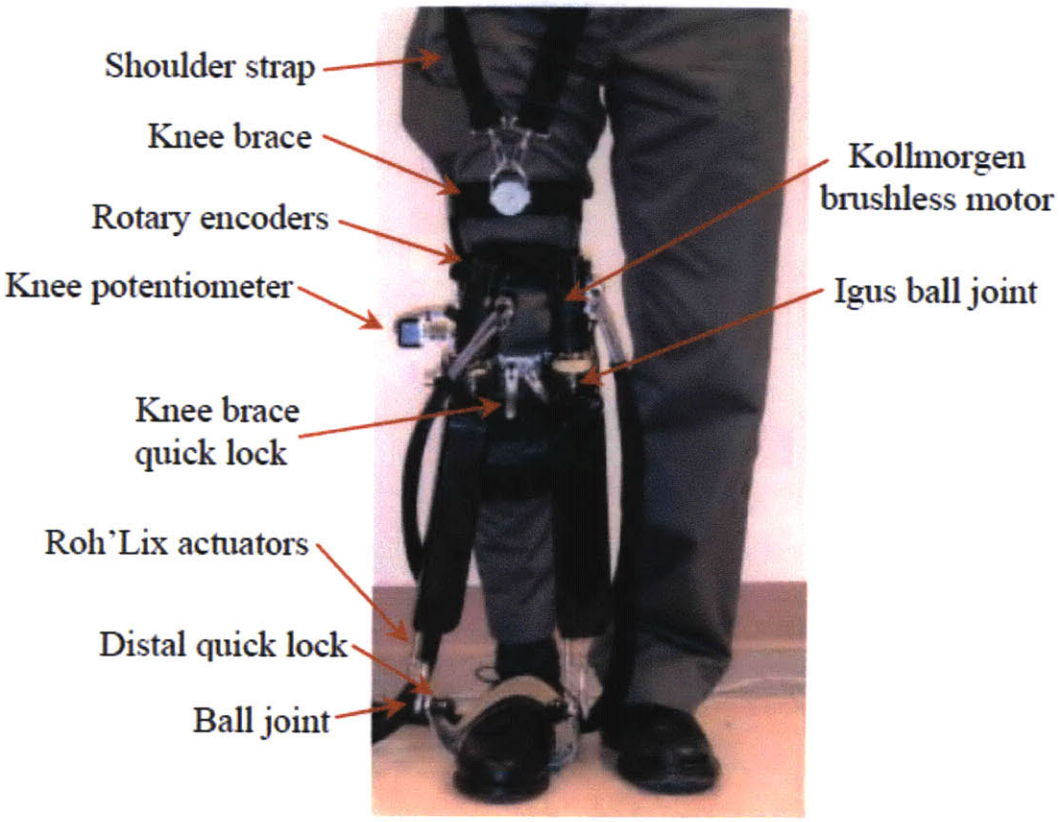

Figure 5: Photograph of an individual wearing the Anklebot in the standing position. When used in the sitting position, the knee joint is affixed to a chair to ensure that the motion of the ankle is isolated and that the foot will not hit the chair or floor [10].

For this experiment, the Anklebot was used in both the sitting position and while walking on the treadmill. During sitting, the Anklebot was used to measure the maximum velocity of voluntary movements of the ankle in various directions.

During walking, the Anklebot was used to measure the velocity of the ankle for slow, natural, and fast cadence.

3.2 Clock Program

Several computer tools were developed to use in conjunction with the Anklebot for rehabilitation purposes. One tool, the "clock" program, instructs the user to make motions in specific directions. As pictured in Figure 6, the clock program consists of a circle divided into a variable number of pie slices, with smaller circles in the center and at the edge of each pie slice. Each pie slice represents a direction of motion. The pie slices in the vertical direction represent the dorsi/plantarflexion direction of motion. The pie slices in the horizontal direction represent the inversion/eversion direction of motion. The slices on the diagonal represent a mixture of motions in the 2 directions.

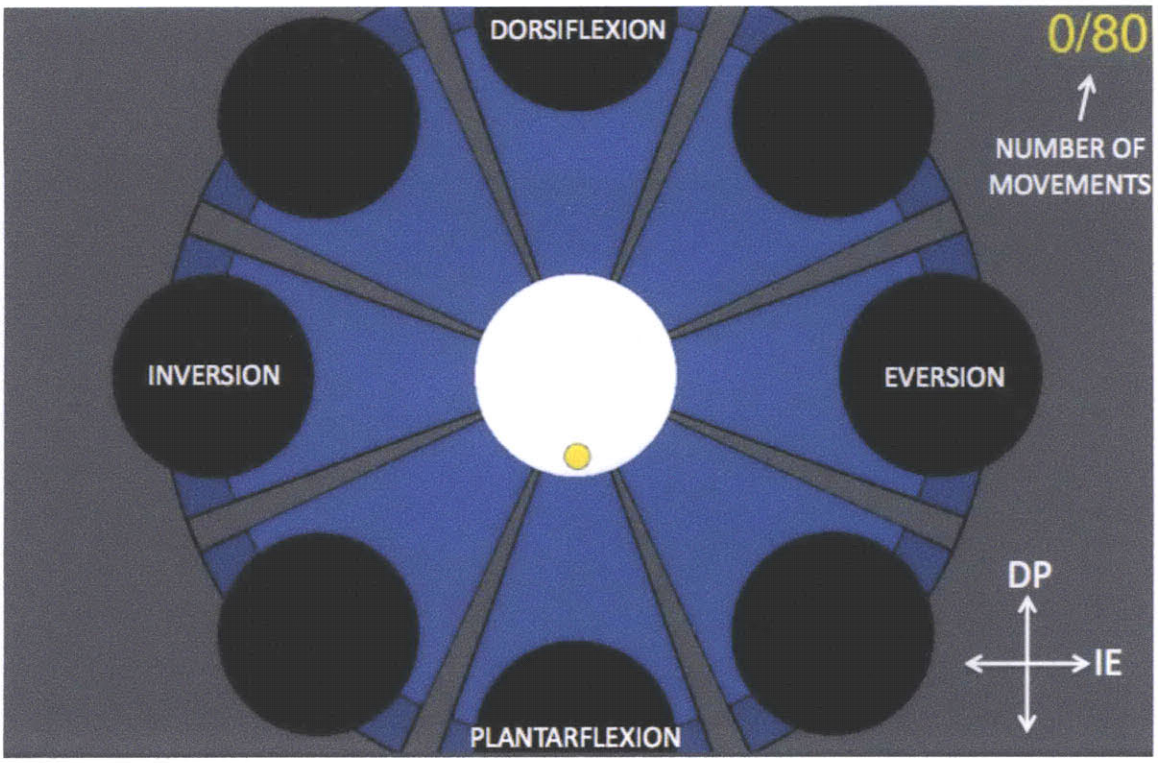

Figure 6: Screenshot of the clock program used to guide subject through ankle motions in 8 different directions. The number in the top right represents the number of movements performed out of the total of 80 per trial.

The yellow dot in the center represents the current position of the ankle. When the dot is in the center of the circle, it is in the anatomical neutral position, which was calibrated to be at the subject's neutral ankle position while sitting. For each requested motion, one of the outer circles changed color until the yellow dot representing the ankle position passed through the area of that circle. Then the center circle lit up until the yellow circle crossed its borders. This process repeated in each of the eight directions five times, in a random order, for a total forty motions away from the center of the circle and forty towards the center of the circle. The clock program allowed several parameters to be adjusted, including the size of each target, the number of targets, the resistance or assistance provided by the Anklebot,

as well as many other parameters not adjusted for this experiment. The program also synchronized EMG data with the position data taken during each trial.

The clock program was used in this experiment to instruct the subject to make voluntary ankle motions in various directions. Because the aim of the experiment was to measure speed, not accuracy, the targets were set to a large diameter to minimize the subject's concern about missing the target. Also, the resistance of the Anklebot was set to zero, as was the assistance it provided, so that the subject could move as naturally as possible with minimal encumbrance. The order of movements was randomized so as to prevent muscles from tiring too quickly.

3.3 Procedures

Three (1 male, 2 female) healthy subjects participated after they had given informed consent. The subjects' height, weight, and body-mass index are summarized in Table 1.

Table 1: Summarizes height, weight, and body-mass index for each of the three subjects.

	Height [m]	Weight [kg]	Body-mass Index [kg/m^2]
Subject A	1.68	61.2	21.7
Subject B	1.57	59.0	23.9
Subject C	1.73	71.2	23.9

To begin, EMG sensors were attached to the subject's anterior tibialis, peroneus longus, and gastrocnemius using two-sided tape. We chose not to measure soleus activity. The Delsys EMG sensors used have a gain of 1000x and bandwidth of 20-

450Hz. The placement of each sensor was tested using an oscilloscope to ensure a strong signal before attaching the sensor with tape. The subject was seated and assisted into the Anklebot's knee brace, the brace attached to the chair, and the Anklebot attached to the brace. The subject was then introduced to the clock program. The subject was instructed to move their foot as quickly as possible and not to be concerned about accuracy or reaction time. Subjects were told to wait until they knew in which direction they would move next before starting the movement. After practicing with the program until the subject felt comfortable, two trials of forty movements away from center, for a total of 10 in each direction, were performed and recorded.

Next, the knee brace was disconnected from the chair to allow the subject to move to the treadmill. The subject was then asked to walk at a self-selected speed slower than their normal gait. The Anklebot was used to record EMG and joint angular position and velocity for 30 seconds. The subject then adjusted the treadmill speed to a pace that felt natural, and data was recorded for 30 seconds. Finally, the subject was asked to adjust the speed to a self-selected pace that was faster than normal, but slow enough that they felt comfortable wearing the Anklebot. Data was recorded for 30 seconds at this speed.

4.0 RESULTS

4.1 Summary of Results

Two trials of the maximum voluntary speed test were performed per subject, with five movements per trial in each of the eight directions indicated in Figure 6.

The average and standard deviation of maximum dorsiflexion and plantarflexion velocities for each subject during the voluntary motion test are listed in Table 2, along with the average and standard deviation of maximum dorsiflexion and plantarflexion velocities obtained during a 30 second walk trial.

Table 2: Summarizes maximum dorsiflexion and plantarflexion velocities attained by each subject both voluntarily and while walking.

	Voluntary Dorsiflexion Velocity [deg/sec]	Walking Dorsiflexion Velocity [deg/sec]	Voluntary Plantarflexion Velocity [deg/sec]	Walking Plantarflexion Velocity [deg/sec]
Subject A	87±28	92±8	83±26	205±17
Subject B	59±14	181±30	56±18	215±20
Subject C	175±17	140±34	213±31	218±15

For the voluntary trial, the velocity is the average over 10 trials (5 for each of the 2 voluntary motion test trials) of the peak velocity. For the walking trial, the velocity is the average of the peak velocity in each stride over the 30-second trial. The number of strides varied with speed, as shown in Table 3. Each of the three subjects walked for 30 seconds at each of three speeds. Speeds are listed in Table 3, normalized by height to show that subjects are taking approximately the same number of steps in the 30 second trials, assuming that stride length is directly correlated to height.

Table 3: Treadmill speeds chosen by each subject, normalized by subject height and resulting number of strides per trial. One trial was performed at each speed for 30 seconds.

	Slow Speed [mph/ft]	# of Strides (slow)	Normal Speed [mph/ft]	# of Strides (normal)	Fast Speed [mph/ft]	# of Strides (fast)
Subject A	0.251	18	0.376	20	0.573	21
Subject B	0.252	24	0.348	24	0.484	23
Subject C	0.282	29	0.406	27	0.618	29

The dorsiplantar (DP) component of velocity in each of the 8 directions was averaged and is summarized in Figure 7. The inversion and eversion velocities were not analyzed for this paper.

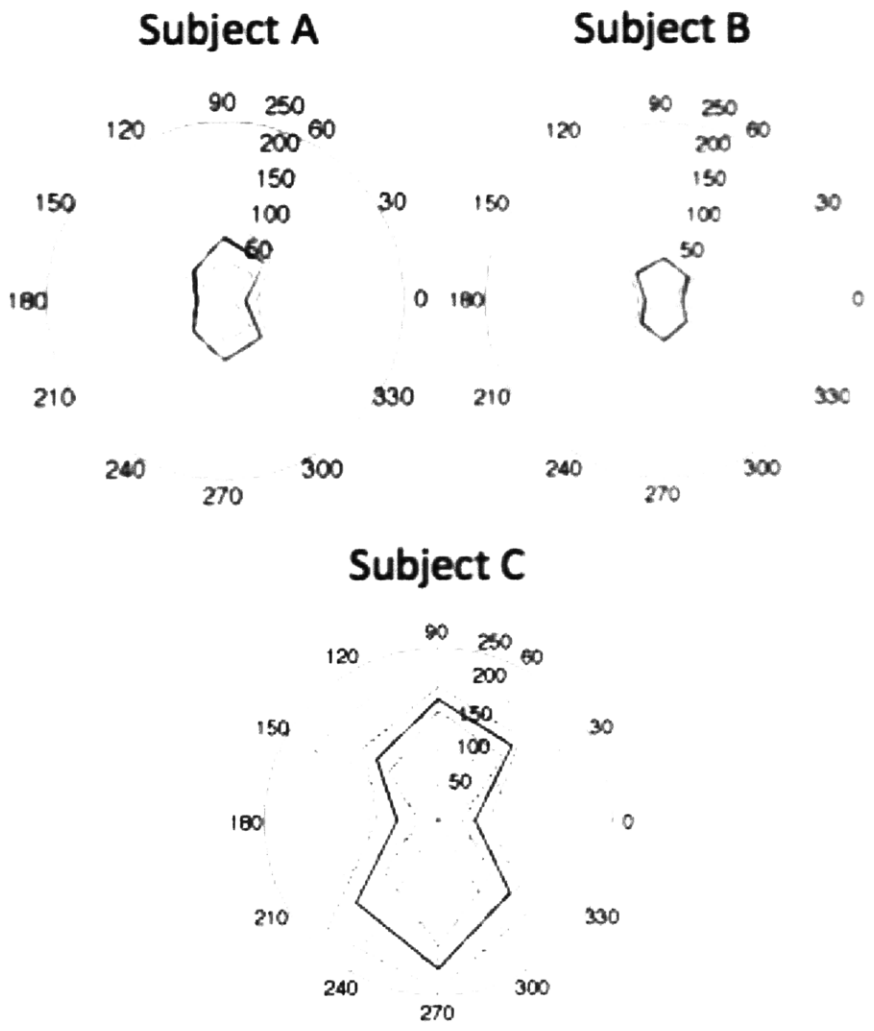

Figure 7: The solid line represents DP average velocity of 10 trials over each of the 8 directions tested for each of 3 subjects. Dashed lines show plus/minus 1 standard deviation.

From **Figure 7**, it is clear that each of the 3 subjects exhibited the same trends in DP velocity magnitudes, as indicated by the similar shape of each of the 3 plots. Yet, the magnitudes of the velocities vary widely between subjects.

A characteristic plot of the DP velocity versus time is shown in Figure 8. Peak dorsiflexion velocity always occurs directly following toe-off, and peak plantarflexion velocity always occurs directly following heal strike.

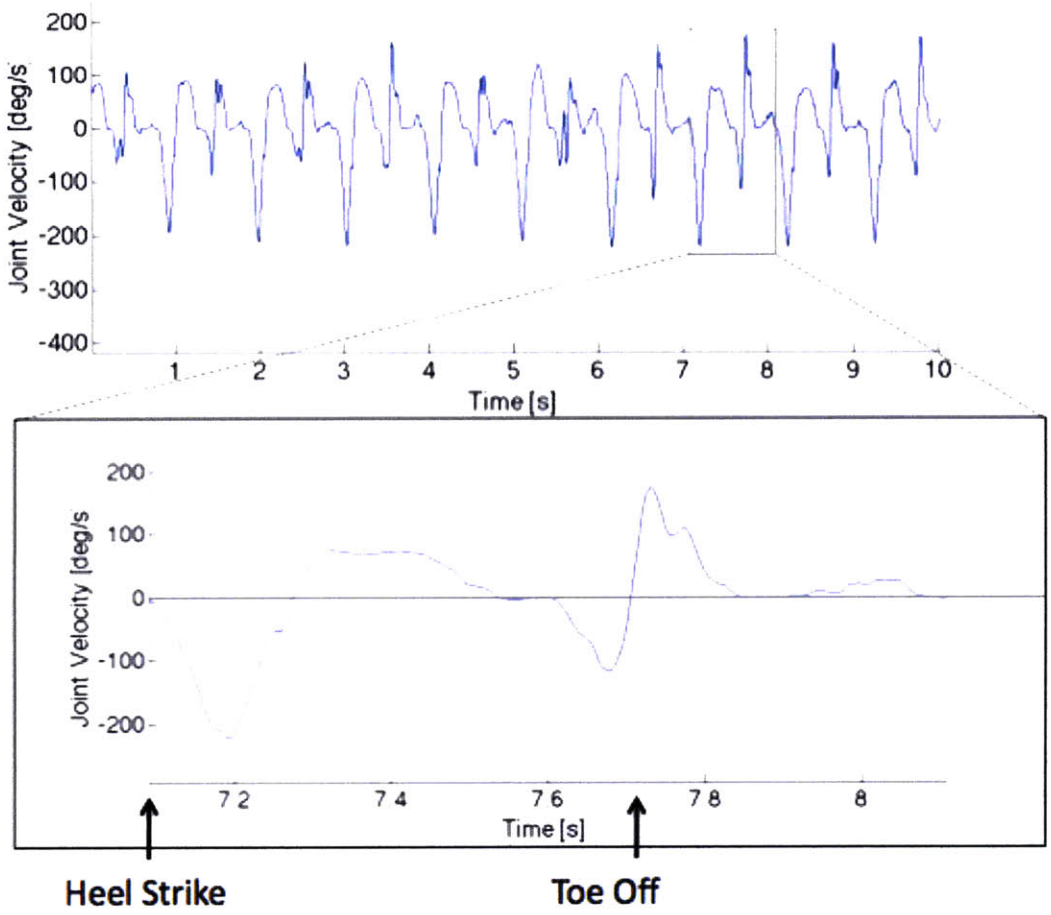

Figure 8: Characteristic DP velocity profile while walking on a treadmill. The points of heel strike and toe off are indicated in the lower plot.

To test the variability in the velocity between strides for each subject, the position of the ankle was plotted against the ankle angular velocity at that position. The plots for each subject at slow, normal, and fast speeds are shown in Figure 9, Figure 10, and Figure 11, respectively. These figures show a remarkable variation in walking styles between subjects. Walking styles become more uniform as walking speed increases.

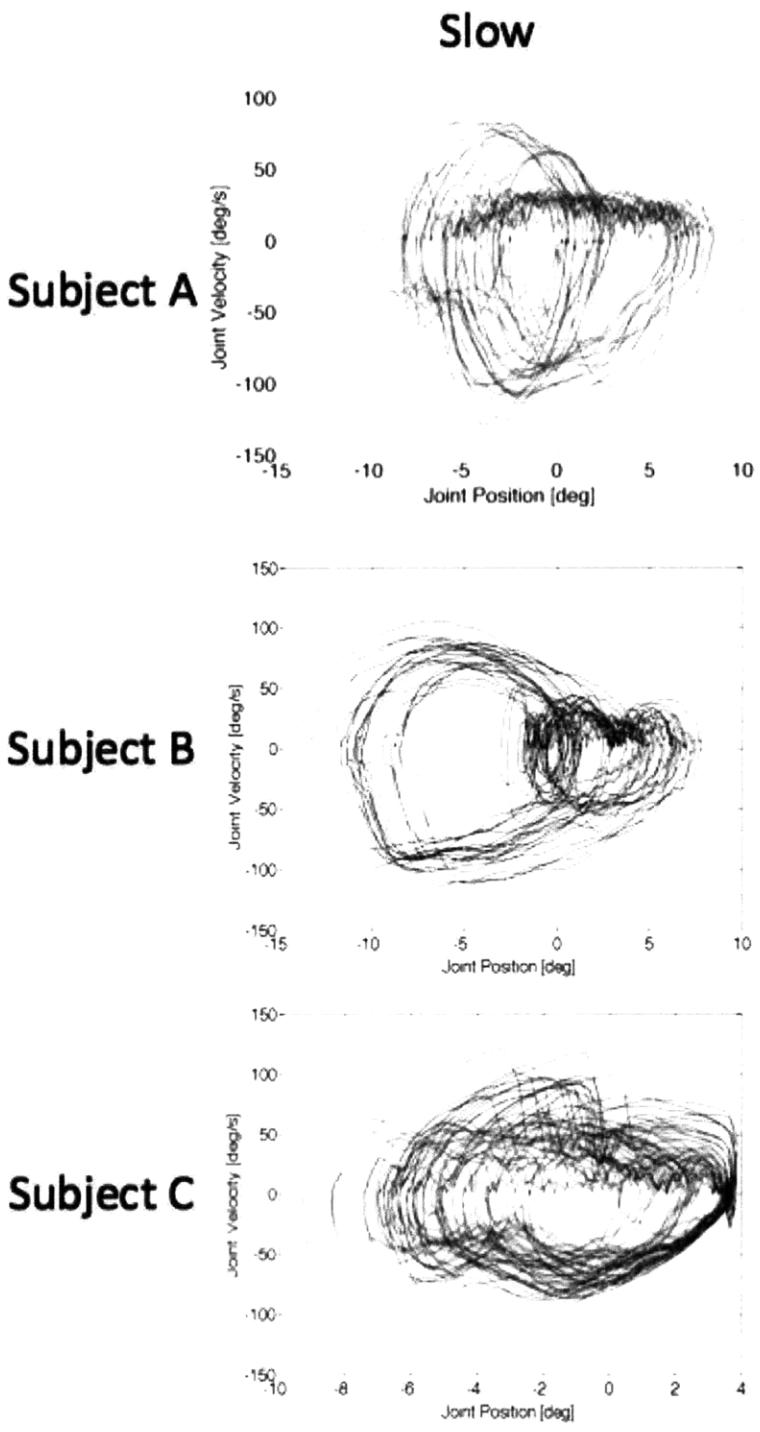

Figure 9: DP velocity as a function of position during 30-second walk trial at slow speed.

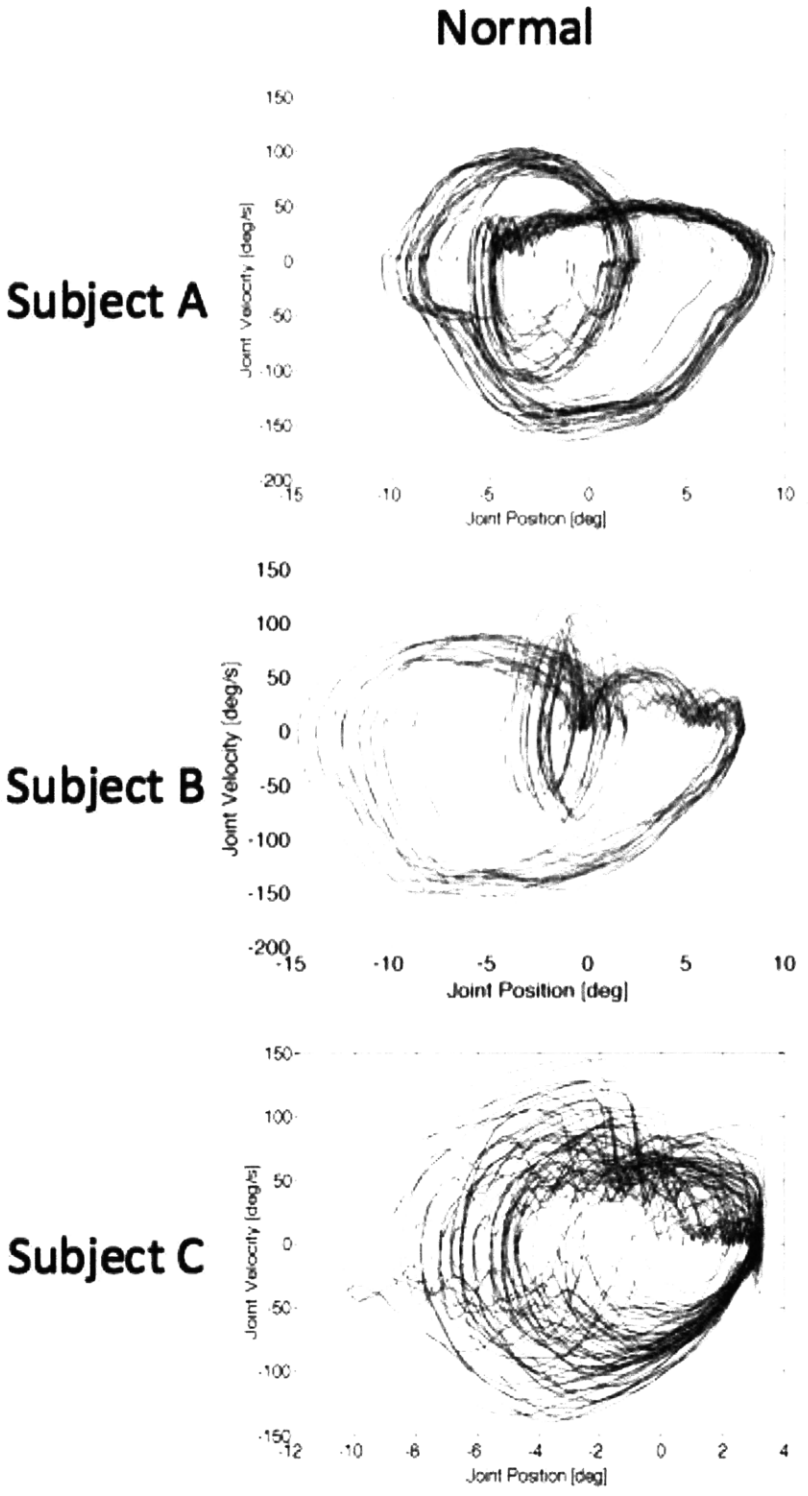

Figure 10: DP velocity as a function of position during 30-second walk trial at normal speed.

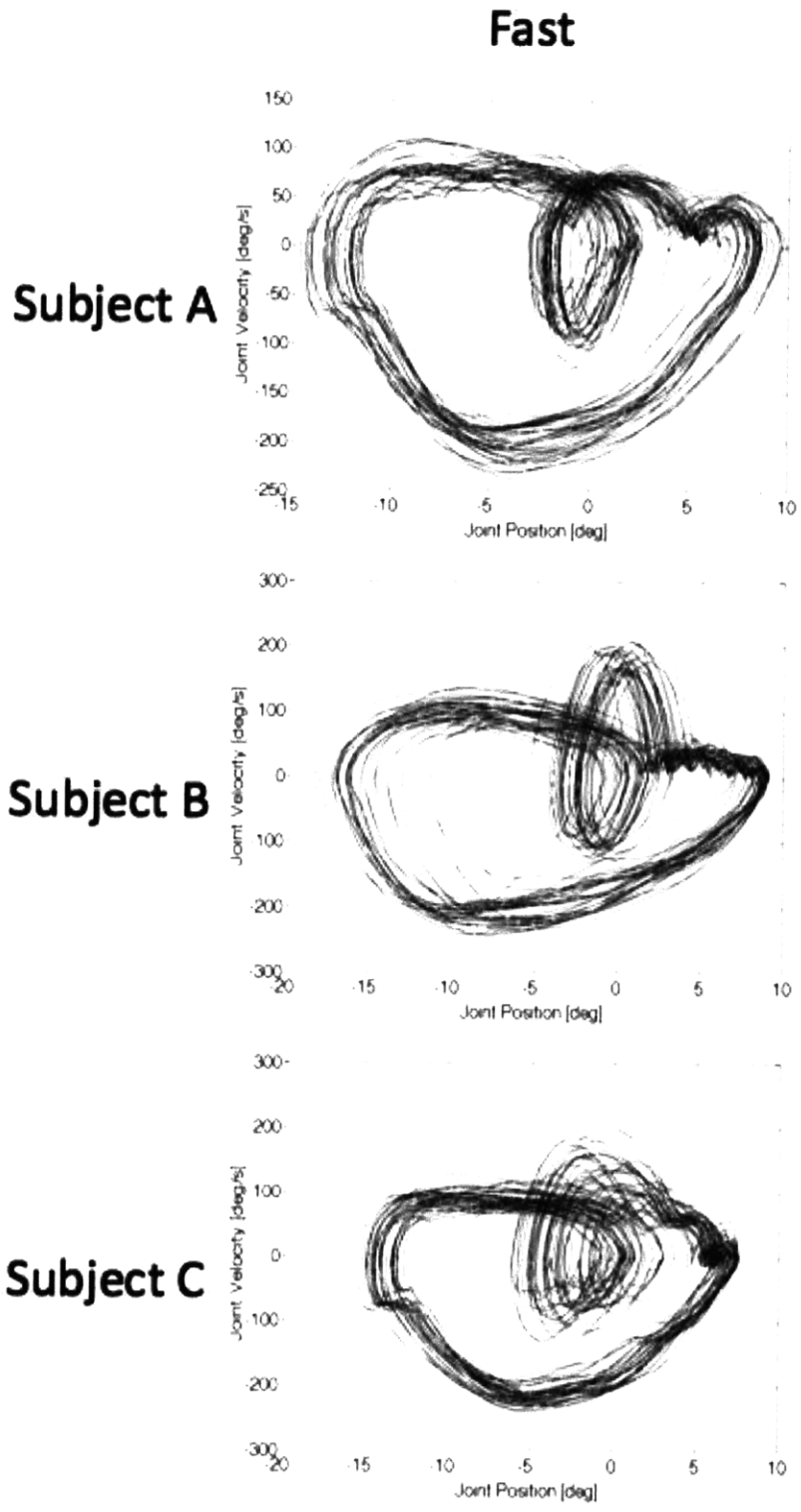

Figure 11: DP velocity as a function of position during 30-second walk trial at fast speed.

The peak ankle velocities in the dorsiflexion and plantarflexion directions during the walking trials for each speed and subject were identified and averaged. Results are summarized in Table 4.

Table 4: Summarizes average and standard deviation of peak ankle velocities in dorsiflexion and plantarflexion directions during walking trials at each of the 3 speeds.

	Slow Walk Dorsiflexion Velocity [deg/s]	Normal Walk Dorsiflexion Velocity [deg/s]	Fast Walk Dorsiflexion Velocity [deg/s]	Slow Walk Plantarflexion Velocity [deg/s]	Normal Walk Plantarflexion Velocity [deg/s]	Fast Walk Plantarflexion Velocity [deg/s]
Subject A	75±12	92±9	87±16	97±18	146±10	205±17
Subject B	79±13	88±23	181±30	95±10	141±12	211±20
Subject C	89±18	103±23	140±34	79±10	110±18	218±15

Figure 12 shows the average peak dorsiflexion velocity and the average peak plantarflexion velocity at each speed. These values are plotted alongside the maximum voluntary DP velocities in each compass direction. Comparing the two will indicate whether the dorsiflexion and plantarflexion motions made while walking are voluntarily generated by muscle action or are due to the mechanics of foot-ground interaction.

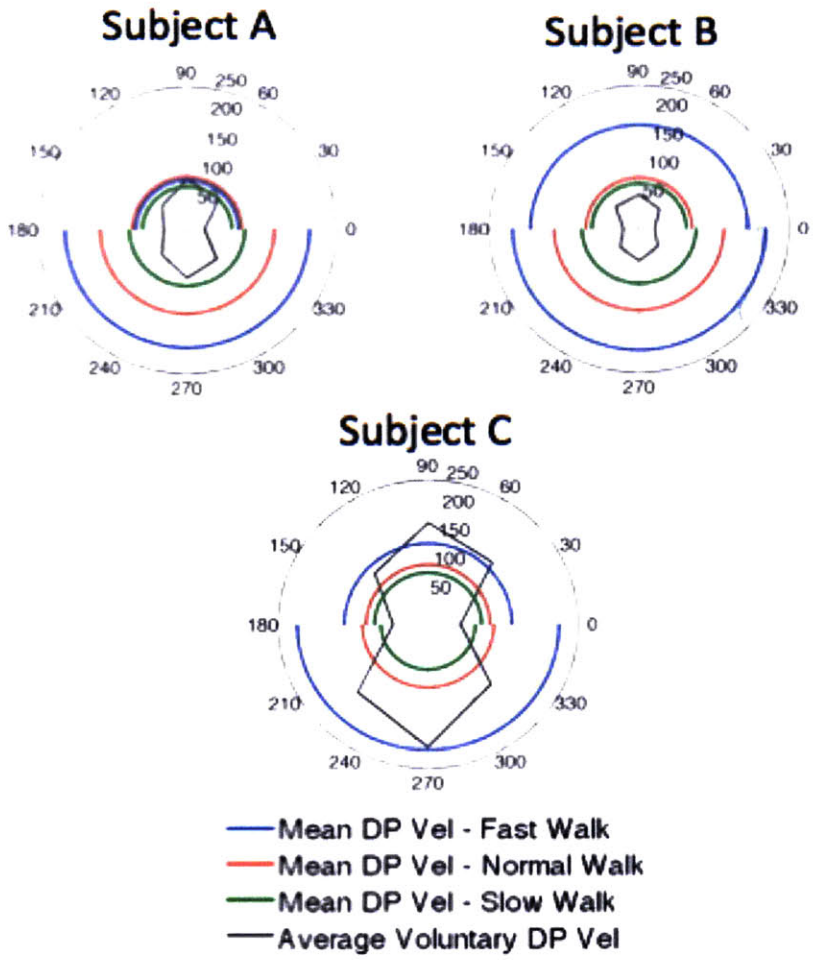

Figure 12: Average DP Velocity at each speed of walking plotted on top of average maximum voluntary DP velocity in each compass direction.

In Figure 12, you can see that the plantarflexion velocity during walking is much greater than during voluntary movement for subjects A and B. Results are less clear for subject C. The dorsiflexion velocity during walking is greater than during voluntary movement for subject B, essentially the same for subject A and smaller for subject C.

In order to determine when critical muscles are firing relative to the peak DP velocities, the root mean square (RMS) of the raw EMG signals were plotted next to DP velocities during walking and voluntary movements. RMS of raw EMG signal

was found using the Matlab script outlined in Appendix A. Unfortunately, many of the EMG results show only the artifact of 60Hz noise and did not pick up on any electrical muscle signals, thus are excluded from this paper. This result may be due to improper grounding. Figure 13 shows the EMG of the gastrocnemius muscle during 1 step while walking at a fast pace. Figure 14 shows the EMG of the anterior tibialis muscle during dorsiflexion of the voluntary motion for subjects A and C. The EMG signal is scaled by a factor of 1000 in order to compare its shape to that of the DP velocity curves. The peroneus longus EMG was not examined because it relates to inversion and eversion, which were not covered in this report. It is important to note that the RMS of the EMG changes much more slowly than the ankle motion due to the result of rectifying the signal. In filtering out the higher frequency noise, the resultant curve responds more slowly than the original signal.

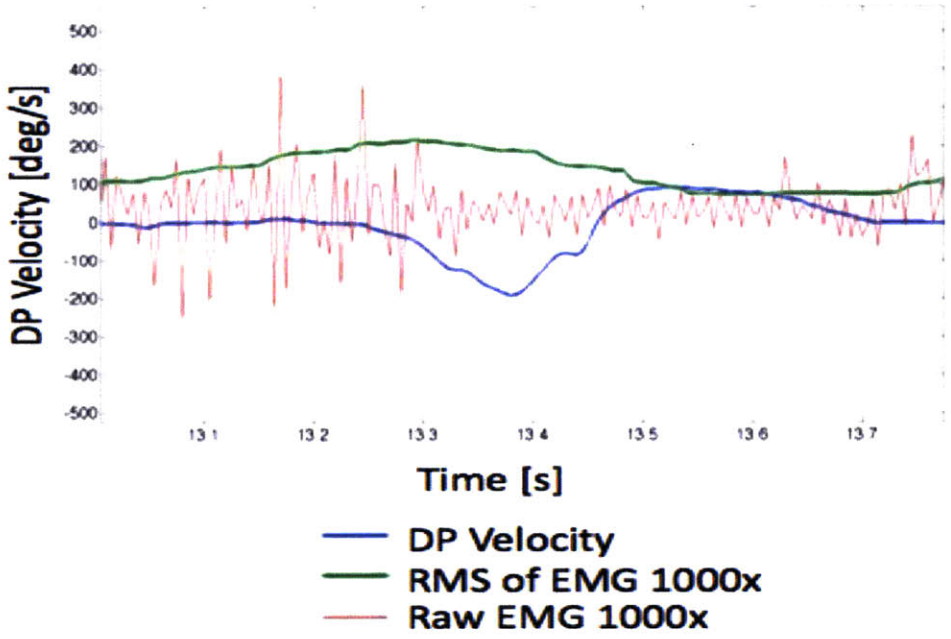

Figure 13: DP velocity, raw EMG, and rectified EMG signal of gastrocnemius muscle for subject C during fast walking test.

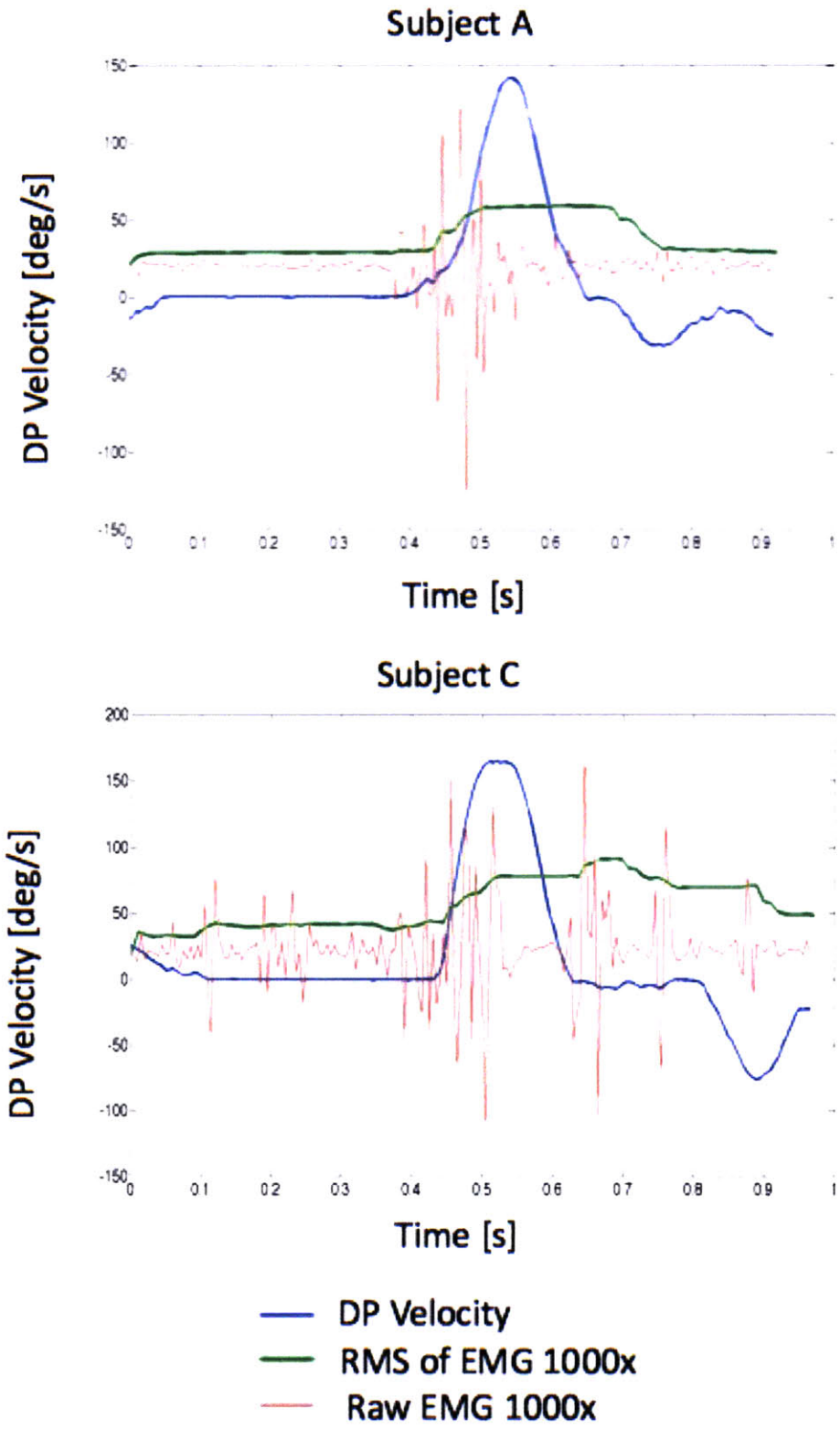

Figure 14: DP velocity, raw EMG, and rectified EMG signal of anterior tibialis for subjects A and C during dorsiflexion of the voluntary motion test.

4.2 Discussion

Comparing the results from the voluntary motion test and the walking test shown in Figure 12, a few key observations stand out. For all three subjects, the mean of the peak plantarflexion speed was higher for walking than during voluntary motion, even though the latter was nominally made as fast as possible. For subjects A and B, there was a large difference between mean peak plantarflexion velocity during walking and during the voluntary motion test. Subject C's mean peak speed was closer in the two cases. One explanation for the slower voluntary speeds exhibited by subjects A and B may be that they were too focused on the accuracy of their motion, despite being told that the accuracy was not important. A t-test performed using Matlab's ttest2 function on the voluntary motion and walking data for each case showed that all differences between voluntary motion and walking were statistically significant with 95% confidence with the exception of the plantarflexion velocities of subject C. The difference between the plantarflexion velocity while walking and during voluntary motion for subject C is not statistically significant. For subjects A and B, it appears that voluntary motion alone cannot account for the ankle kinematics observed during walking. Instead, ankle motion is due, at least in part, to mechanical interaction between the foot and ground, mediated by ankle mechanical impedance. For subject C, it is possible that the subject was capable of walking faster and that walking at a faster pace may have shown similar results to the other 2 subjects.

Results for the dorsiflexion direction were less clear. Figure 12 shows that the mean of the peak speed reached during the voluntary motion test was greater than

that during walking for subjects A and C. One important aspect to note, though, is that subjects in the voluntary motion test were trying to move as fast as they could, whereas in the walking test, they were not walking as fast as possible. Also, subject B seemed to have the most trouble ignoring accuracy while performing the voluntary motion test. This may explain why the DP velocities for this subject are much smaller than for the other subjects.

In Figure 12, it is interesting to note that for subject A, the mean peak dorsiflexion velocity was greater when walking at a normal speed than during fast walking. This suggests that the subject altered their gait pattern to accommodate the faster pace, as indicated by the difference between the velocity versus position curves shown in Figure 10 and Figure 11.

Figure 9, Figure 10, and Figure 11 shed a little more light on the difference in walking styles between the three subjects. As the walking speed increased, the plots tended to become more defined and less variable, especially for subject C. For subject A, the fast walking data is slightly different than for the other two subjects; the small "inner loop" stays completely within the "outer loop". The "inner loop" represents the portion of gait from plantarflexion during stance to dorsiflexion immediately following toe-off. For subjects B and C, the "inner loop" intersects the "outer loop," indicating higher dorsiflexion velocity after toe-off than during stance phase. This difference in walking styles may explain why subject A displayed a higher mean peak dorsiflexion velocity for normal walking than for fast walking.

In order to better understand the relative contribution of voluntary muscle activation and the mechanics of foot-ground interaction, EMG signals of selected

muscles were compared to the velocity profiles. Figure 14 shows the anterior tibialis EMG signal for subjects A and C during the voluntary motion test. In both cases, there is a clear spike in anterior tibialis muscle activity just prior to the start of motion. Figure 13 shows the gastrocnemius EMG signal for 1 step in subject C's fast walking test. There is a clear spike in gastrocnemius activity just prior to heel strike. It was shown earlier that the plantarflexion motion after heel strike is due, at least in part, to foot-ground interactions, independent of flexion of the gastrocnemius. It could be inferred that the gastrocnemius contraction seen in Figure 13 may be coupled with a co-contraction of the anterior tibialis, increasing the impedance of the ankle in preparation for heel strike. Further testing needs to be done with properly calibrated EMG sensors in order to confirm this speculation.

4.3 Conclusion and Recommendations

The results of this experiment showed that the ankle plantarflexion that occurs after heel strike cannot be a voluntary motion generated exclusively by the contraction of the muscles that plantarflex the foot. This is consistent with the ankle acting primarily as a shock-absorber during heel-strike. For the dorsiflexion following toe off, the results were less clear. Further tests should be done at faster walking speeds to determine whether the foot will dorsiflex faster during that stage than in the voluntary speed test. Also, the clock program, although modified to mitigate the need for accuracy, still seemed to distract some subjects from the goal of pure speed. A better test may be to use the Anklebot while sitting and instruct

the subject to move the foot up or down. Without the visual feedback, they won't be distracted by whether the move was accurately executed.

There is also a very distinct difference in walking forms between the subjects. A further study into these differences may provide further insight into the control of the ankle during walking.

REFERENCES:

[1] http://www.ninds.nih.gov/disorders/foot_drop/foot_drop.htm

[2] Developing World Prosthetics Lecture (02/25/2009) given by H. Herr.

[3] Di Gregorio, A. Leardini, J.J. O'Connor, V. Parenti-Castell. *Mathematical models of passive motion at the human ankle joint by equivalent spatial parallel mechanisms.* Med Bio Eng Comput, 2007, 45:305-313.

[4] Dul, G.E. Johnson. *A kinematic model of the human ankle.* J Biomed Eng , 1985, Vol. 7, April, 137-143.

[5] Cailliet, R. *Foot and Ankle Pain*, Second edition, Davis co., Philadelphia, 1983.

[6] Scott, S.H. and Winter, D.A. *Biomechanical Model of the human foot: kinematics and kinetics during stance phase of walking.* J Biomechanics, 1993, Vol. 26, No. 9, 1091-1104.

[7] Giacomozzi, C. et al. *Measurement device for ankle joint kinematic and dynamic characterization.* Med. Biol. Eng. Comput., 2003, 41, 486-493.

[8] Winter, D.A. *Overall principle of lower limb support during stance phase of gait.* J Biomechanics, 1980, 13, 923-927.

[9] Winter, D.A. *Biomechanical motor patterns in normal walking.* J Motor Behavior, 1983, Vol. 15, No. 4, 302-330.

[10] Roy, A. et al. *Robot-aided neurorehabilitation: a novel robot for ankle rehabilitation,* 2008.

[11] Gailey, R. et al. *Review of secondary physical conditions associated with lower-limb amputation and long-term prosthesis use.* Journal of Rehabilitation Research & Development, 2008, Vol. 45, No. 1, 15-30.

APPENDIX A: Matlab script to obtain RMS of raw EMG signal

```
%This function finds the moving RMS of a signal over an
integral window
%using various numerical integration techniques. It can
also plot the
%signal together with the envelope estimate
%
%It is intended for use in estimating the amplitude of an
EMG signal.
%
%It is possible to select from the trapezoid rule and
Simpson's 1/3rd rule
%in numerical integration
%
%Simpson's is more accurate, but the trapezoid rule is fast
and possibly
%could be used in real time through a modification of this
function
%
%By Patrick Ho

function RMS=AmplitudeEstimator(sampleemg, window, Hz,
method, doplot)
%INPUT: signal, moving frame in seconds, sample rate,
integration method
%method = 1 %is trapezoid rule which consumes one point per
step
%method = 2 %is simpson's 1/3 rule which consumes 2 points
per step
%Hz=1000;    %1000Hz refresh rate
%window=.05; %This is 50ms.
%doplot == 1 means plot the results.

integral_window=floor(window*Hz/method); %Steps in integral
window. The method unit accounts for the number of points
used per estimate
signallength=length(sampleemg);
h=method/Hz; % #steps / (steps/second) = duration of time
step


if method == 1
   I=zeros(1,signallength);
   for a=2:signallength
       I(a)=h*(sampleemg(a-1)^2+sampleemg(a)^2)/2;
   end
   cuml=zeros(1,signallength);
```

```
    cuml(1)=I(1);
    RMS=zeros(1,signallength);
    RMS(1)=sqrt(cuml(1)/h);
    for b=2:(integral_window)
         cuml(b)=cuml(b-1)+I(b);
         RMS(b)=sqrt(cuml(b)/(b*h));
    end
    for b=(integral_window+1):length(I)
         cuml(b)=cuml(b-1)+I(b)-I(b-integral_window);
         RMS(b)=sqrt(cuml(b)/window);
    end
end


if method == 2

     I=zeros(1,ceil(signallength/2));

     for a=1:floor(signallength/2-1)
         I(a)=simpson13(h,sampleemg(a*2-1)^2,
sampleemg(a*2)^2, sampleemg(a*2+1)^2); %Integral of square
of function
     end

     cuml=zeros(1,length(I)); %cumulative integral
     cuml(1)=I(1);
     RMS=zeros(1,length(I)); %RMS value
     RMS(1)=sqrt(cuml(1)/h/2); %cumulative integral needs to
be divided by the integral window)
     for b=2:(integral_window)
         cuml(b)=cuml(b-1)+I(b);
         RMS(b)=sqrt(cuml(b)/(b*h));
     end

     for b=(integral_window+1):length(I)
         cuml(b)=cuml(b-1)+I(b)-I(b-integral_window);
         RMS(b)=sqrt(cuml(b)/window);
     end
end

if doplot == 1
     signaltime=linspace(0,signallength/Hz,signallength);
     RMStime=linspace(h/2,signallength/Hz-h/2,length(RMS));
     %figure
     %plot(RMS)
     figure
     plot(signaltime,sampleemg,'g',RMStime,RMS,'r')
end
```

APPENDIX B: Matlab script to analyze raw data

```
%This program will load data from an anklebot output file
and place it into
%a data structure called "data"
%You can access individual fields by writing
data.'fieldname'

clear all; close all;
%Write the folder that your data is in here
cd('/Users/jzimmerman/Documents/MIT/Spring
2009/Thesis/nstrials/walktrial')

Fs = 200;
ndirs = 8;
mag_th = 20;

%Write your filename here
[data,emg]=getData('fast1.asc')

for i=1:data.J
    time(i)=(i-1)/Fs;
end

data.dp_pos=data.dp_pos-mean(data.dp_pos);
data.dp_vel=data.dp_vel-mean(data.dp_vel);
figure(1)
plot(time, data.dp_vel*180/pi,'-b') %Velocity profile for
walking trial
xlabel('Time [s]')
ylabel('Joint Velocity [deg/s]')
title('fast.asc')
figure(2)
plot(data.dp_pos*180/pi,data.dp_vel*180/pi,'-k') %Position
versus velocity
xlabel('Joint Position [deg]')
ylabel('Joint Velocity [deg/s]')
figure(3)
%velocity, Raw AT EMG, and RMS of AT EMG
plot(time,data.dp_vel*180/pi,time,1000*data.emg_ch1,emg.t1,
1000*emg.ch1)
figure(4)
%velocity, Raw gastroc EMG, and RMS of gastroc EMG
plot(time,data.dp_vel*180/pi,time,1000*data.emg_ch3,emg.t3,
1000*emg.ch3)
```

```
%
% Find Maximum DP velocity for voluntary movement
%

cd('/Users/jzimmerman/Documents/MIT/Spring
2009/Thesis/nstrials/trial1/')

n=getData('Nt22.asc');

maxdpn(1)=max(n.dp_vel);
for i=1:n.J
    t1(i)=(i-1)/200;
end

n=getData('Nt24.asc');
maxdpn(2)=max(n.dp_vel);
for j=1:n.J
    t2(j)=(j-1)/200;
end

[n emgx]=getData('Nt27.asc');
maxdpn(3)=max(n.dp_vel);
for i=1:n.J
    t3(i)=(i-1)/200;
end
figure(5)
% Voluntary dorsiflexion, AT Raw EMG, AT RMS of EMG
plot(t3,180/pi*n.dp_vel,emgx.t1,1000*emgx.ch1,t3,n.emg_ch1*
1000)
xlabel('Time [s]')
ylabel('DP Velocity [deg/s]')

n=getData('Nt29.asc');
maxdpn(4)=max(n.dp_vel);
for i=1:n.J
    t4(i)=(i-1)/200;
end

ne=getData('NEt17.asc');
maxdpne(1)=max(ne.dp_vel);

ne=getData('NEt21.asc');
maxdpne(2)=max(ne.dp_vel);

ne=getData('NEt28.asc');
filein = 'NEt28.asc';
maxdpne(3)=max(ne.dp_vel);
```

```
ne=getData('NEt36.asc');
maxdpne(4)=max(ne.dp_vel);

nw=getData('NWt12.asc');
maxdpnw(1)=max(nw.dp_vel);

nw=getData('NWt14.asc');
maxdpnw(2)=max(nw.dp_vel);

nw=getData('NWt31.asc');
maxdpnw(3)=max(nw.dp_vel);

nw=getData('NWt38.asc');
maxdpnw(4)=max(nw.dp_vel);

nw=getData('NWt7.asc');
maxdpnw(5)=max(nw.dp_vel);

s=getData('St13.asc');
mindps(1)=min(s.dp_vel);

s=getData('St15.asc');
mindps(2)=min(s.dp_vel);

s=getData('St40.asc');
mindps(3)=min(s.dp_vel);

s=getData('St8.asc');
mindps(4)=min(s.dp_vel);

[s emgx]=getData('St9.asc');
mindps(5)=min(s.dp_vel);
for j=1:s.J
    tt5(j)=(j-1)/200;
end
figure(6)
% Voluntary plantarflexion, gastroc Raw EMG, gastroc RMS of
EMG
plot(tt5,180/pi*s.dp_vel,emgx.t3,1000*emgx.ch3,tt5,s.emg_ch
3*1000)

se=getData('SEt19.asc');
mindpse(1)=min(se.dp_vel);

se=getData('SEt1.asc');
mindpse(2)=min(se.dp_vel);
```

```
se=getData('SEt25.asc');
mindpse(3)=min(se.dp_vel);

se=getData('SEt26.asc');
mindpse(4)=min(se.dp_vel);

se=getData('SEt4.asc');
mindpse(5)=min(se.dp_vel);

sw=getData('SWt10.asc');
mindpsw(1)=min(sw.dp_vel);

sw=getData('SWt30.asc');
mindpsw(2)=min(sw.dp_vel);

sw=getData('SWt34.asc');
mindpsw(3)=min(sw.dp_vel);

sw=getData('SWt6.asc');
mindpsw(4)=min(sw.dp_vel);

e=getData('Et11.asc');
maxdpe(1)=max(e.dp_vel);
mindpe(1)=min(e.dp_vel);

e=getData('Et18.asc');
maxdpe(2)=max(e.dp_vel);
mindpe(2)=min(e.dp_vel);

e=getData('Et23.asc');
maxdpe(3)=max(e.dp_vel);
mindpe(3)=min(e.dp_vel);

e=getData('Et33.asc');
maxdpe(4)=max(e.dp_vel);
mindpe(4)=min(e.dp_vel);

e=getData('Et35.asc');
maxdpe(5)=max(e.dp_vel);
mindpe(5)=min(e.dp_vel);

w=getData('Wt16.asc');
maxdpw(1)=max(w.dp_vel);
mindpw(1)=min(w.dp_vel);

w=getData('Wt20.asc');
maxdpw(2)=max(w.dp_vel);
mindpw(2)=min(w.dp_vel);
```

```
w=getData('Wt37.asc');
maxdpw(3)=max(w.dp_vel);
mindpw(3)=min(w.dp_vel);

w=getData('Wt5.asc');
maxdpw(4)=max(w.dp_vel);
mindpw(4)=min(w.dp_vel);

cd('/Users/jzimmerman/Documents/MIT/Spring
2009/Thesis/nstrials/trial2/')

n=getData('Nt18.asc');
maxdpn(5)=max(n.dp_vel);

n=getData('Nt20.asc');
maxdpn(6)=max(n.dp_vel);

n=getData('Nt23.asc');
maxdpn(7)=max(n.dp_vel);

n=getData('Nt36.asc');
maxdpn(8)=max(n.dp_vel);

ne=getData('NEt15.asc');
maxdpne(5)=max(ne.dp_vel);

ne=getData('NEt16.asc');
maxdpne(6)=max(ne.dp_vel);

ne=getData('NEt26.asc');
maxdpne(7)=max(ne.dp_vel);

ne=getData('NEt34.asc');
maxdpne(8)=max(ne.dp_vel);

nw=getData('NWt17.asc');
maxdpnw(6)=max(nw.dp_vel);

nw=getData('NWt19.asc');
maxdpnw(7)=max(nw.dp_vel);

nw=getData('NWt21.asc');
maxdpnw(8)=max(nw.dp_vel);

nw=getData('NWt27.asc');
maxdpnw(9)=max(nw.dp_vel);
```

```
nw=getData('NWt37.asc');
maxdpnw(10)=max(nw.dp_vel);

s=getData('St13.asc');
mindps(6)=min(s.dp_vel);

s=getData('St25.asc');
mindps(7)=min(s.dp_vel);

s=getData('St30.asc');
mindps(8)=min(s.dp_vel);
filein = 'Sb40.asc';

s=getData('St5.asc');
mindps(9)=min(s.dp_vel);

s=getData('St6.asc');
mindps(10)=min(s.dp_vel);

se=getData('SEt31.asc');
mindpse(6)=min(se.dp_vel);

se=getData('SEt40.asc');
mindpse(7)=min(se.dp_vel);

se=getData('SEt4.asc');
mindpse(8)=min(se.dp_vel);

se=getData('SEt7.asc');
mindpse(9)=min(se.dp_vel);

se=getData('SEt8.asc');
mindpse(10)=min(se.dp_vel);

sw=getData('SWt14.asc');
mindpsw(5)=min(sw.dp_vel);

sw=getData('SWt22.asc');
mindpsw(6)=min(sw.dp_vel);

sw=getData('SWt28.asc');
mindpsw(7)=min(sw.dp_vel);

sw=getData('SWt33.asc');
mindpsw(8)=min(sw.dp_vel);

sw=getData('SWt9.asc');
mindpsw(9)=min(sw.dp_vel);
```

```
e=getData('Et12.asc');
maxdpe(6)=max(e.dp_vel);
mindpe(6)=min(e.dp_vel);

e=getData('Et24.asc');
maxdpe(7)=max(e.dp_vel);
mindpe(7)=min(e.dp_vel);

e=getData('Et29.asc');
e.dp_vel = e.file(:,5);
maxdpe(8)=max(e.dp_vel);
mindpe(8)=min(e.dp_vel);

e=getData('Et38.asc');
maxdpe(9)=max(e.dp_vel);
mindpe(9)=min(e.dp_vel);

w=getData('Wt10.asc');
maxdpw(5)=max(w.dp_vel);
mindpw(5)=min(w.dp_vel);

w=getData('Wt11.asc');
maxdpw(6)=max(w.dp_vel);
mindpw(6)=min(w.dp_vel);

w=getData('Wt1.asc');
maxdpw(7)=max(w.dp_vel);
mindpw(7)=min(w.dp_vel);

w=getData('Wt35.asc');
maxdpw(8)=max(w.dp_vel);
mindpw(8)=min(w.dp_vel);

figure(7)
%polar plot of dp magnitudes in each direction
rho=180/pi*[mean(maxdpn),mean(maxdpne),abs(mean(mindpe)),ab
s(mean(mindpse)),abs(mean(mindps)),abs(mean(mindpsw)),mean(
maxdpw),mean(maxdpnw),mean(maxdpn)];
rho2=180/pi*[mean(maxdpn)+std(maxdpn),mean(maxdpne)+std(max
dpne),abs(mean(mindpe))+abs(std(mindpe)),abs(mean(mindpse))
+abs(std(mindpse)),...

abs(mean(mindps))+abs(std(mindps)),abs(mean(mindpsw))+abs(s
td(mindpsw)),mean(maxdpw)+std(maxdpw),mean(maxdpnw)+std(max
dpnw),mean(maxdpn)+std(maxdpn)];
rho3=180/pi*[mean(maxdpn)-std(maxdpn),mean(maxdpne)-
std(maxdpne),abs(mean(mindpe))-
```

```
abs(std(mindpe)),abs(mean(mindpse))-abs(std(mindpse)),...
    abs(mean(mindps))-abs(std(mindps)),abs(mean(mindpsw))-
abs(std(mindpsw)),mean(maxdpw)-std(maxdpw),mean(maxdpnw)-
std(maxdpnw),mean(maxdpn)-std(maxdpn)];
theta=[pi/2,pi/4,0,-pi/4,-pi/2,-3*pi/4,pi,3*pi/4,pi/2];
td = 0:.01:pi;
tp = pi:.01:2*pi;
x=zeros(1, length(td));
for i=1:1:length(td)
    x(i)=1;
end
% walking peak DP velocities
Dpeakslow = [59.1 82.5 95.1 93.5 99 66.4 84.7 117.5 66.7
121.8 102.2 81.6 63.7 97.1 92.2 98.1 88.2 59.7 96.1 99.5
109];
mslow = mean(Dpeakslow);
Dpeakmed = [92 93.1 58.4 107.5 79.3 96.2 106.9 100.7 112.6
85.6 106.6 126.6 145 146.4 114.1 99.7 64.5 73.8 105.7 128.2
128.7 85.2 121];
mmed = mean(Dpeakmed);
Dpeakfast = [107 93.7 125.6 163 99.9 94.4 157.9 175.8 161.4
171.5 117.3 210.7 146.7 183.1 199 161.6 116.5 135.3 100.9
150.7 89.4 145.2 156.4 185.8 112.3 114.6 136.2 96.8 139.5];
mfast = mean(Dpeakfast);
Ppeakslow = [83.4 74.8 73.1 75.4 59.2 69.4 65.9 87.4 81.6
69.1 85.4 89.1 86.4 81.3 101.6 74.2 63.4 84.4 86.6];
mslowp = mean(Ppeakslow);
Ppeakmed = [88.62 102.9 97.8 123.9 83.4 89.3 111.8 89.7
115.3 103.3 96.9 105.5 135.1 134 117 96.3 123.2 83.5 114.3
122.6 139.7 138.6 109.3];
mmedp = mean(Ppeakmed);
Ppeakfast = [193.3 212.1 222.2 200 211.9 224.3 221.8 221
218.8 259.7 202.2 216.6 191.9 216.4 229.3 208.2 232.1 227.7
236.5 218.8 239.6 225.3 212.2 218.5 211.9 229.8 199.2 230
193.1];
mfastp = mean(Ppeakfast);
%polar plot of average peak dp velocities in each direction
polar(tp,mfastp*x,'-b')
hold on;
polar(tp,mmedp*x,'-r')
polar(tp,mslowp*x,'-g')
polar(theta,rho,'-k')
polar(theta,rho2,'--k')
polar(theta,rho3,'--k')
polar(td,mfast*x,'-b')
polar(td,mmed*x,'-r')
polar(td,mslow*x,'-g')
h = legend('Mean DP Vel - Fast Walk','Mean DP Vel - Normal
```

```
Walk','Mean DP Vel - Slow Walk','Average Voluntary DP
Vel',4);
set(h,'Interpreter','none')
figure(8)
rho4 =
180/pi*[max(maxdpn),max(maxdpne),abs(min(mindpe)),abs(min(m
indpse)),abs(min(mindps)),abs(min(mindpsw)),max(maxdpw),max
(maxdpnw),max(maxdpn)];
%polar plot of maximum peak dp velocities in each direction
polar(tp,max(Ppeakfast)*x,'-b')
hold on;
polar(tp,max(Ppeakmed)*x,'-r')
polar(tp,max(Ppeakslow)*x,'-g')
polar(theta,rho4,'k')
polar(td,max(Dpeakfast)*x,'-b')
polar(td,max(Dpeakmed)*x,'-r')
polar(td,max(Dpeakslow)*x,'-g')
q = legend('Max DP Vel - Fast Walk','Max DP Vel - Normal
Walk','Max DP Vel - Slow Walk','Max Voluntary DP Vel',4);
set(q,'Interpreter','none')

%statistical t-test
TTEST(1) = ttest2(-180/pi*maxdpn,Dpeakfast);
TTEST(2) = ttest2(-180/pi*mindps,Ppeakfast);



cd('/Users/jzimmerman/Documents/MIT/Spring
2009/Thesis/nstrials')
```

APPENDIX C: Matlab script to read in raw data

```
function [data,emg]=getData(dFile)
filein = dFile;
data.file = load([filein]);
data.i = data.file(:,1);
data.J = length(data.i);
data.ie_pos = data.file(:,2);
data.dp_pos = data.file(:,3);
data.ie_vel = data.file(:,4);
data.dp_vel = data.file(:,5);
data.ie_torque = data.file(:,6);
data.dp_torque = data.file(:,7);
data.emg_ch1 = data.file(:,15);
data.emg_ch2 = data.file(:,16);
data.emg_ch3 = data.file(:,17);
data.emg_ch4 = data.file(:,18);
emg.ch1=AmplitudeEstimator(data.emg_ch1,.25,200,2,0);
emg.ch2=AmplitudeEstimator(data.emg_ch2,.25,200,2,0);
emg.ch3=AmplitudeEstimator(data.emg_ch3,.25,200,2,0);
emg.ch4=AmplitudeEstimator(data.emg_ch4,.25,200,2,0);
emg.t1=linspace(0,length(data.ie_pos)/200,length(emg.ch1));
emg.t2=linspace(0,length(data.ie_pos)/200,length(emg.ch2));
emg.t3=linspace(0,length(data.ie_pos)/200,length(emg.ch3));
emg.t4=linspace(0,length(data.ie_pos)/200,length(emg.ch4));
```